Bifurcation of pulsation instability in one-dimensional H_2-O_2 detonation with detailed reaction mechanism

Wenhu Han,[1,2,*] Wenjin Ma,[1] Chengeng Qian,[1] Jennifer Wen,[2] and Cheng Wang[1,*]
[1]*State Key Laboratory of Explosion Science and Technology, Beijing Institute of Technology, Beijing 100081, China*
[2]*School of Engineering, University of Warwick, Coventry CV4 7AL, United Kingdom*

(Received 29 January 2019; published 29 October 2019)

Classical modes of one-dimensional (1D) detonation characterized by a simplified reaction model are reproduced by using a real chemical kinetics for the H_2-O_2 system with argon dilution. As Ar dilution is varied, the bifurcation points of pulsating instability are identified and a formed bifurcation diagram is compared with that obtained by the one-step reaction model. Eventually, the numerical results demonstrate that, for real detonations with detailed chemistry, the criterion of Ng *et al.* works well on prediction of the 1D detonation instability. Furthermore, the detonability limits are found respectively at low and high Ar dilutions. Above the high Ar dilution limit, detonations decays to the minimum level where long autoignition time and small heat release rate make reestablishment impossible for both 1D and 2D simulations. However, below the low Ar dilution limit, a 1D detonation cannot be sustained due to high instability, while the corresponding cellular detonation can propagate sustainably due to the role of transverse instability.

DOI: 10.1103/PhysRevFluids.4.103202

I. INTRODUCTION

A detonation wave manifests pulsations in one dimension [1] and cellular instability in multiple dimensions [2–5], depending on the initial conditions and mixture properties. For a pulsating detonation near the Chapman-Jouguet (CJ) state, extensive experiments and theoretical analyses have observed longitudinal oscillation of the detonation front [6–11]. Specially, the theoretical studies of Clavin and Williams [2,3,12] have milestone significance for the physical explanation of origin of one-dimensional (1D) instability and the relation of pulsating and cellular instabilities. He and Lee [13] examined the 1-D instability of detonation and demonstrated that 1-D detonations in planar geometry are classified into three classes through identifying the boundary of detonation stability and observing different modes of shock oscillation: neutral stability, pulsation with a single-mode oscillation and with multiperiod mode, and highly nonlinear and even chaotic oscillations. Sharpe and Falle [14] observed a series of failures followed by reignition for a highly unstable detonation with a large activation energy and found the cause of instabilities in the reaction zone by using a one-step overall reaction. Romick, Aslam, and Powers [15] studied the effect of diffusion on the dynamics of unsteady detonations with a one-step overall reaction, and found that diffusion influenced strongly the dynamics of unstable detonation. Ng *et al.* [16] examined the study of 1D detonation using a two-step reaction model and proposed a universal criterion for 1D detonation instability by defining a stability factor, and gave the bifurcation diagram of a pulsating detonation.

*Corresponding authors: hanwenhu@bit.edu.cn; wangcheng@bit.edu.cn

A three-step chain-branching reaction model was used to predict the detonability limit by Short and Quirk [17]. As the studies of chemical reaction kinetics are advanced, realistic chemistry is used to calculate the stability of 1D detonations. Radulescu *et al.* [18] used a seven-step chemistry model to simulate 1D detonation propagation in an acetylene-oxygen mixture and investigated the effect of argon dilution in stabilizing detonations. Yungster and Radhakrishnan [19] investigated the high-frequency and small-amplitude pulsation for overdriven detonations supported by a piston and revealed the effect of initial pressure on pulsating mode. Romick, Aslam, and Powers [20] used a detailed H_2-air mechanism to establish a bifurcation diagram of peak shock pressure with the change in overdriven factor determined by a piston velocity through calculation of the 1D viscous detonation with a supporting piston [21,22]. Sussman [23] simulated pulsating detonations by using a detailed H_2-air mechanism, concluding that the pulsating propagation depends on the ratio of heat release time to induction time. In general, however, the studies of 1D detonations with real chemistry have been few for pulsating instability of detonations globally close to CJ state.

The present work aims to examine the propagation mode of 1D detonation driven by real chemistry and to give the pulsation bifurcation diagram for the H_2-O_2-Ar system. In the following we shall first state the governing equations and the numerical method, and then present and discuss the results.

II. GOVERNING EQUATIONS

The governing equations are the one-dimensional, reactive, compressible Navier-Stokes (NS) equations:

$$\frac{\partial \rho}{\partial t} + \frac{\partial \rho u}{\partial x} = 0, \tag{1}$$

$$\frac{\partial \rho u}{\partial t} + \frac{\partial (\rho u^2 + p - \tau)}{\partial x} = 0, \tag{2}$$

$$\frac{\partial \rho E}{\partial t} + \frac{\partial \rho u E + (p - \tau)u + q}{\partial x} = 0, \tag{3}$$

$$\frac{\partial \rho Y_i}{\partial t} + \frac{\partial \rho u Y_i + \zeta_i}{\partial x} = \bar{W}_i \dot{\omega}_i, \quad i = 1, \ldots, N-1, \tag{4}$$

$$E = h + \frac{p}{\rho} + \frac{u^2}{2}, \tag{5}$$

$$p = \sum_{i=1}^{N} \rho Y_i R_i T = \rho \left(\sum_{i=1}^{N} Y_i R_i \right) T, \quad R_i = \frac{R_u}{\bar{W}_i}, \tag{6}$$

$$h = \sum_{i=1}^{N} Y_i h_i, \tag{7}$$

$$h_i(T) = h_i^f + \int_{T_0}^{T} c_{p,i}(\hat{T}) d\hat{T}, \tag{8}$$

where p, ρ, E, T, u, h are the pressure, the density, the total energy per unit mass, the temperature, the x velocities, and the enthalpy per unit mass; $Y_1, \ldots, Y_N$ is the mass fraction of ith species, with $\sum_{i=1}^{N} Y_i = 1$; W_i, R_i, c_{pi}, and h_i^f are the molecular weight, the specific gas constant, the specific heat, and the enthalpy of formation of ith species, and $R_u = 8.31\,\mathrm{J/(mol\,K)}$ is the universal gas constant.

To close the system, constitutive relations are specified for an ideal mixture of N species:

$$\tau = \frac{4\mu\partial u}{3\partial x}, \tag{9}$$

$$\zeta_i = -\frac{D_i^T \partial T}{T\partial x} + \rho \sum_{\substack{k=1 \\ k\neq i}}^{N} \frac{\bar{W}_i D_{ik} X_k}{\bar{W}} \left(\frac{1}{X_k}\frac{\partial X_k}{\partial x}\right) + \left(1 - \frac{\bar{W}_k}{\bar{W}}\right)\frac{1}{p}\frac{\partial p}{\partial x}, \tag{10}$$

$$q = -\kappa\frac{\partial T}{\partial x} + \sum_{i=1}^{N} \zeta_i h_i - R_u T \sum_{i=1}^{N} \frac{D_i^T}{\bar{W}_i}\left[\frac{1}{X_i}\frac{\partial X_i}{\partial x} + \left(1 - \frac{\bar{W}_i}{\bar{W}}\right)\frac{1}{p}\frac{\partial p}{\partial x}\right], \tag{11}$$

$$X_i = \frac{\bar{W}}{\bar{W}_i} Y_i, \tag{12}$$

$$\bar{W} = \left(\sum_{i=1}^{N} \frac{Y_i}{\bar{W}_i}\right)^{-1}, \tag{13}$$

where $\bar{W}$ is the mixture molecular mass, D_{ik} the multicomponent diffusion coefficient between the ith and kth species, D_i^T the thermal diffusion coefficient of the ith species, T the temperature, μ the dynamic viscosity of the mixture, κ the thermal conductivity of the mixture, and $X_1, \ldots, X_N$ are the mole fractions of species i, with $\sum_{i=1}^{N} X_i = 1$. The mixture properties are evaluated using the CHEMKIN [24] and TRANSPORT [25] packages. We adopt the San Diego mechanism [26] which comprises the eight species H_2, O_2, OH, O, H, H_2O, HO_2, and H_2O_2.

III. NUMERICAL METHOD

The semidiscretization of governing Eqs. (1)–(4) is as follows:

$$\frac{dU}{dt} = H_a(U) + H_d(U) + H_s(U), \tag{14}$$

where $H_a(U)$, $H_d(U)$, and $H_s(U)$ are approximations of advection term, diffusion term, and reaction source term, respectively. The numerical flux $\hat{F}_{a,i+1/2}$ in the advection term $H_a(U) = -\frac{\hat{F}_{a,i+1/2} - \hat{F}_{a,i-1/2}}{\Delta x}$ is obtained with fifth-order WENO reconstruction [27] as presented in the following. The physical flux $\boldsymbol{F}_a$ can be divided by using Lax-Friedrichs flux splitting,

$$\boldsymbol{F}_a^{\pm} = \tfrac{1}{2}(F_a \pm \alpha U), \tag{15}$$

where $\alpha = \max|\lambda|$ and λ are the eigenvalues of Jacobian Matrix for $\boldsymbol{F}_a$.

For simplicity, we only present the reconstruction of numerical flux $\hat{\boldsymbol{F}}^{+}_{a,i+1/2}$, which is an approximation of $\boldsymbol{F}^{+}_{a,i+1/2}$. The fifth-order numerical flux is given by

$$\hat{\boldsymbol{F}}^{+}_{a,i+1/2} = \sum_{r=0}^{2} \omega_r F^{+,(r)}_{a,i+1/2}, \tag{16}$$

where the third-order numerical fluxes on three small stencils are given by

$$\hat{\boldsymbol{F}}^{+,(0)}_{a,i+1/2} = \tfrac{1}{3}F^{+}_{i-2} - \tfrac{7}{6}F^{+}_{i-1} + \tfrac{11}{6}F^{+}_{i}, \tag{17}$$

$$\hat{\boldsymbol{F}}^{+,(1)}_{a,i+1/2} = -\tfrac{1}{6}F^{+}_{i-1} + \tfrac{5}{6}F^{+}_{i} + \tfrac{1}{3}F^{+}_{i+1}, \tag{18}$$

$$\hat{\boldsymbol{F}}^{+,(2)}_{a,i+1/2} = \tfrac{1}{3}F^{+}_{i} + \tfrac{5}{6}F^{+}_{i+1} - \tfrac{1}{6}F^{+}_{i+2}, \tag{19}$$

and the nonlinear weights ω_r are defined as

$$\omega_r = \frac{\alpha_r}{\sum_{s=0}^{2} \alpha_s}, \quad \alpha_r = \frac{d_r}{(\varepsilon + \beta_r)^2} \tag{20}$$

Here the linear weights d_r are given by

$$d_1 = \tfrac{1}{10}, \quad d_2 = \tfrac{3}{5}, \quad d_3 = \tfrac{3}{10}$$

and the smoothness indicators β_r are given by

$$\beta_r = \tfrac{13}{12}(F_{i-2}^{+} - 2F_{i-1}^{+} + F_i^{+})^2 + \tfrac{3}{12}(F_{i-2}^{+} - 2F_{i-1}^{+} + F_i^{+})^2, \tag{21}$$

$$\beta_2 = \tfrac{13}{12}(F_{i-1}^{+} - 2F_i^{+} + F_{i+1}^{+})^2 + \tfrac{3}{12}(F_{i-1}^{+} - F_{i+1}^{+})^2, \tag{22}$$

$$\beta_2 = \tfrac{13}{12}(F_i^{+} - 2F_{i+1}^{+} + F_{i+2}^{+})^2 + \tfrac{3}{12}(3F_i^{+} - 4F_{i+1}^{+} + F_{i+2}^{+})^2, \tag{23}$$

The parameter $\varepsilon = 10^{-6}$ is to ensure that the denominator is not zero. The diffusion term H_d is discretized by the sixth-order central difference scheme.

To solve the stiffness problem, an explicit-implicit additive Runge-Kutta scheme [28] was used in the time discretization. Equation (14) is written as

$$\begin{aligned} \frac{d\boldsymbol{U}}{dt} &= \boldsymbol{H}_{ns}(\boldsymbol{U}) + \boldsymbol{H}_s(\boldsymbol{U}), \\ \boldsymbol{H}_{ns}(\boldsymbol{U}) &= \boldsymbol{H}_a(\boldsymbol{U}) + \boldsymbol{H}_d(\boldsymbol{U}). \end{aligned} \tag{24}$$

The additive Runge-Kutta scheme is used mainly to separate the stiff term $\boldsymbol{H}_s(\boldsymbol{U})$ and nonstiff term $\boldsymbol{H}_{ns}(\boldsymbol{U})$. The explicit Runge-Kutta (ERK) scheme is utilized to integrate $\boldsymbol{H}_{ns}(\boldsymbol{U})$, while $\boldsymbol{H}_s(\boldsymbol{U})$ is handled by the explicit singly diagonally implicit Runge-Kutta (ESDIRK) scheme:

$$\boldsymbol{U}^{(i)} = \boldsymbol{U}^{(n)} + \boldsymbol{X}^{(i)} + (\Delta t) a_{ii}^{[I]} \boldsymbol{H}_s^{(i)}, \quad \boldsymbol{X}^{(i)} = (\Delta t) \sum_{j=1}^{i-1} \left(a_{ij}^{[E]} \boldsymbol{H}_{ns}^{(j)} + a_{ij}^{[I]} \boldsymbol{H}_s^{(j)} \right), \quad i = 2, \ldots, s+1,$$

$$\boldsymbol{U}^{(n+1)} = \boldsymbol{U}^{(n)} + (\Delta t) \sum_{j=1}^{s} \left(b_j^{[E]} \boldsymbol{H}_{ns}^{(j)} + b_j^{[I]} \boldsymbol{H}_s^{(j)} \right), \tag{25}$$

where Δt is the time step size; $\boldsymbol{U}^{(n)}$ is the initial physical value; $\boldsymbol{U}^{(i)}$ is the intermediate physical value; $\boldsymbol{U}^{(n+1)}$ is the final physical value; $a_{ij}^{[E]}$, $a_{ij}^{[I]}$, $b_j^{[E]}$, and $b_j^{[I]}$ are the Butcher coefficients, which are constrained by some accuracy and stability considerations; $\boldsymbol{X}^{(i)}$ is calculated with the given data $\boldsymbol{U}^{(n)}$ explicitly; and $\boldsymbol{H}_s^{(i)}$ and $\boldsymbol{U}^{(i)}$ are calculated by an implicit method for solving nonlinear equations with Newton iteration. The first term of form (11) is developed into

$$\begin{aligned} \boldsymbol{M}\boldsymbol{d}_k^{(i)} &= \boldsymbol{r}_k^{(i)}, \\ \boldsymbol{M} &= \left(\boldsymbol{I} - (\Delta t) a_{ii}^{[I]} \frac{\partial \boldsymbol{H}_s}{\partial \boldsymbol{U}} \bigg|_k \right), \\ \boldsymbol{d}_k^{(i)} &= \left(\boldsymbol{U}^{(i)} - \boldsymbol{U}_k^{(i)} \right), \\ \boldsymbol{r}_k^{(i)} &= -\left(\boldsymbol{U}_k^{(i)} - \boldsymbol{U}^{(n)} \right) + \boldsymbol{X}^{(i)} + (\Delta t) a_{ii}^{[I]} \boldsymbol{H}_s^{(i)} \left(\boldsymbol{U}_k^{(i)} \right), \end{aligned} \tag{26}$$

where subscript k is variable value of the kth iteration; $\boldsymbol{M}$ is the iterative matrix; $\boldsymbol{d}_k^{(i)}$ is the difference between the iterative and real value; and $\boldsymbol{r}_k^{(i)}$ is the remainder value of the iteration equation. When $|\boldsymbol{d}_k^{(i)}| \leqslant \varepsilon$ or $|\boldsymbol{r}_k^{(i)}| \leqslant \varepsilon$, the iteration terminates. The iteration value $\boldsymbol{U}_k^{(i)}$ can be used as $\boldsymbol{U}^{(i)}$, and thereby $\boldsymbol{H}_s^{(i)}$ is calculated with $\boldsymbol{U}^{(i)}$. Finally, the physical value $\boldsymbol{U}^{(n+1)}$ is calculated by the terms of form (25) with $\boldsymbol{H}_s^{(i)}$ and $\boldsymbol{H}_{ns}^{(i)}$.

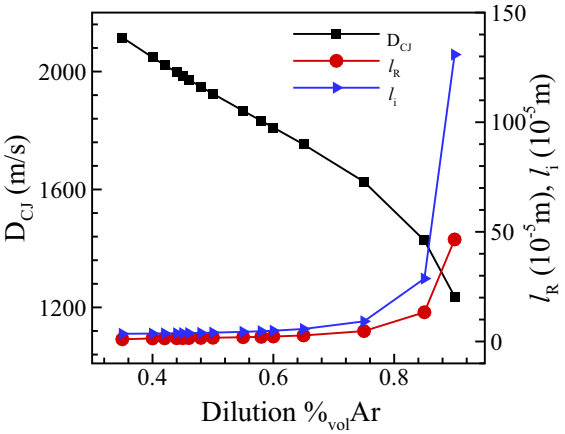

FIG. 1. Induction length, reaction length, and CJ velocity for H_2-O_2 detonations with different argon dilutions at $T_0 = 298$ K and $p_0 = 1$ atm.

The Courant-Friedrichs-Lewy (CFL) number is 0.2 in the simulations. Eventually, the method based on conservation variables was used to solve the equations, which guarantees conservation and also yields good solutions with the shock speed evaluated accurately [29].

IV. RESULTS AND DISCUSSIONS

A. Numerical specifications

The mixture has constant initial pressure and temperature of $p_0 = 1$ atm and $T_0 = 298$ K, respectively. Induction length is defined as the distance from the shock front to the maximum thermicity, while the reaction zone is the length between peak thermicity and the reaction equilibrium. With argon dilution, the change of post-shock temperature T_{VN} is small, with the bounds of $1920 < T_{VN} < 2050$ K for 15%−85%, while it is ∼1491 K for 90% Ar. The corresponding CJ detonation velocity D_{CJ}, the ignition delay time τ, the reaction length l_R, and the induction length l_i as functions of Ar dilution were calculated by CANTERA, as shown in Fig. 1.

The steady Zel'dovich–von Neumann–Döring (ZND) solution including species information is set as the initial condition in the unsteady 1D simulation, and the resulting detonation is allowed to propagate into the mixture at rest to observe the long-time behavior of the detonation propagation. As the overdriven detonation is close to the CJ state, boundary conditions at the piston are then replaced by the condition at the downstream end of the reaction zone, where there is no acoustic wave propagation in the burnt gas directed upstream towards the reaction zone [12]. For freely propagating detonations, disturbance at the rear boundary always is reflected in the laboratory frame. Although it is usually assumed that its influence is small, it is not confirmed whether it changes the dynamics of detonation. To avoid the influence, the rear boundary in the downstream is placed at $x = -0.01$ m and is far enough away from the detonation front so that the solution is not affected by the disturbance from the rear boundary. The value at the CJ state with flow and chemical equilibria is fixed at the rear boundary. The computational domain is 0.12 m and the grid resolution is 60 pts/$l_{1/2}$, where $l_{1/2}$ is half of reaction length, l_R, and corresponds to each Ar dilution, as shown in Fig. 1. The numerical scheme reaches fifth order at the smooth region [29] and hence the grid resolution of 60 pts/$l_{1/2}$ is sufficient to capture detonation structures.

We assess the effect of diffusion on the 1D detonation pulsation. Figure 2 shows the maximum pressure histories of detonations with the NS and Euler equations for 35% Ar and 50% Ar, respectively. It is seen that, for 35% Ar, detonation takes on a highly unstable mode, and the pulsations obtained with the NS and Euler equations have obvious differences in the amplitude

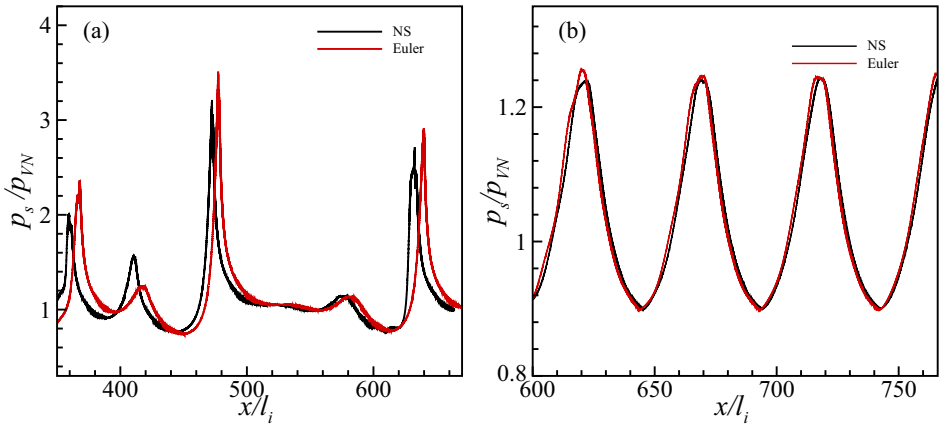

FIG. 2. Maximum pressure histories of 1D detonations with and without diffusion for 35% Ar (a) and 50% Ar (b): p_{VN} is the steady von-Neumann value and p_s is shock pressure.

of oscillations, indicating that diffusion has an obvious effect on the chaotic characteristics. The viscous detonation has smaller amplitude of oscillations than that solved by the Euler equations, which agrees with the findings of Romick, Aslam, and Powers [20]. For 50% Ar, both the NS and Euler equations show almost uniform evolution of single-period pulsation, with small disparity appearing just at peaks of the pulsation. Consequently, this indicates that diffusion plays a role in an unstable detonation, while the influence is minor for the detonation with a single-period mode. Generally, viscosity is minor for a global CJ detonation. Nevertheless, we still use reactive flow NS equations in the following simulations.

From Fig. 3, the detonations with 60 and 120 pts/$l_{1/2}$ are consistent for 35% Ar, with minor difference at the peaks of oscillations. This demonstrates that the present grid resolution is enough to capture the detonation structure. In this result, the numerical scheme can reach fifth order when a smooth initial solution assumed, while it goes back to first order at the discontinuity. In fact, for all numerical schemes, to treat strong discontinuity the order drops to the first order.

B. Propagation modes of 1D detonations for different Ar dilutions

Figure 4 shows typical modes of 1D detonations for different Ar dilutions. It is seen that the high-frequency pulsation appearing in the initial stage oscillates globally and then develops into

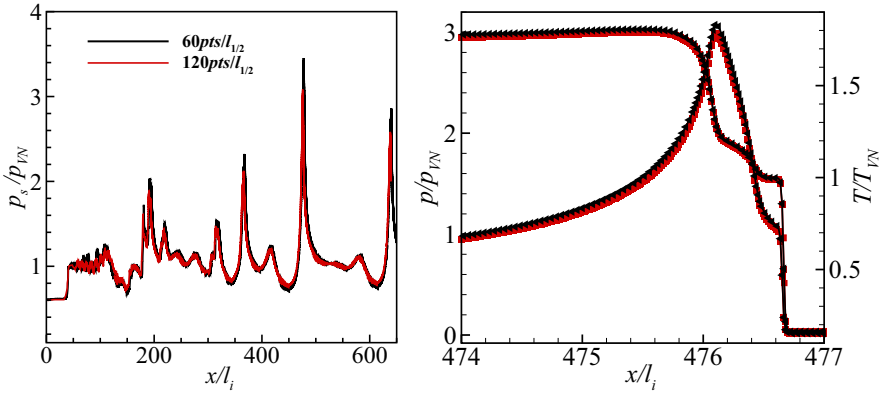

FIG. 3. Maximum pressure histories and detonation structure with 60 and 120 pts/$l_{1/2}$ for 35% Ar.

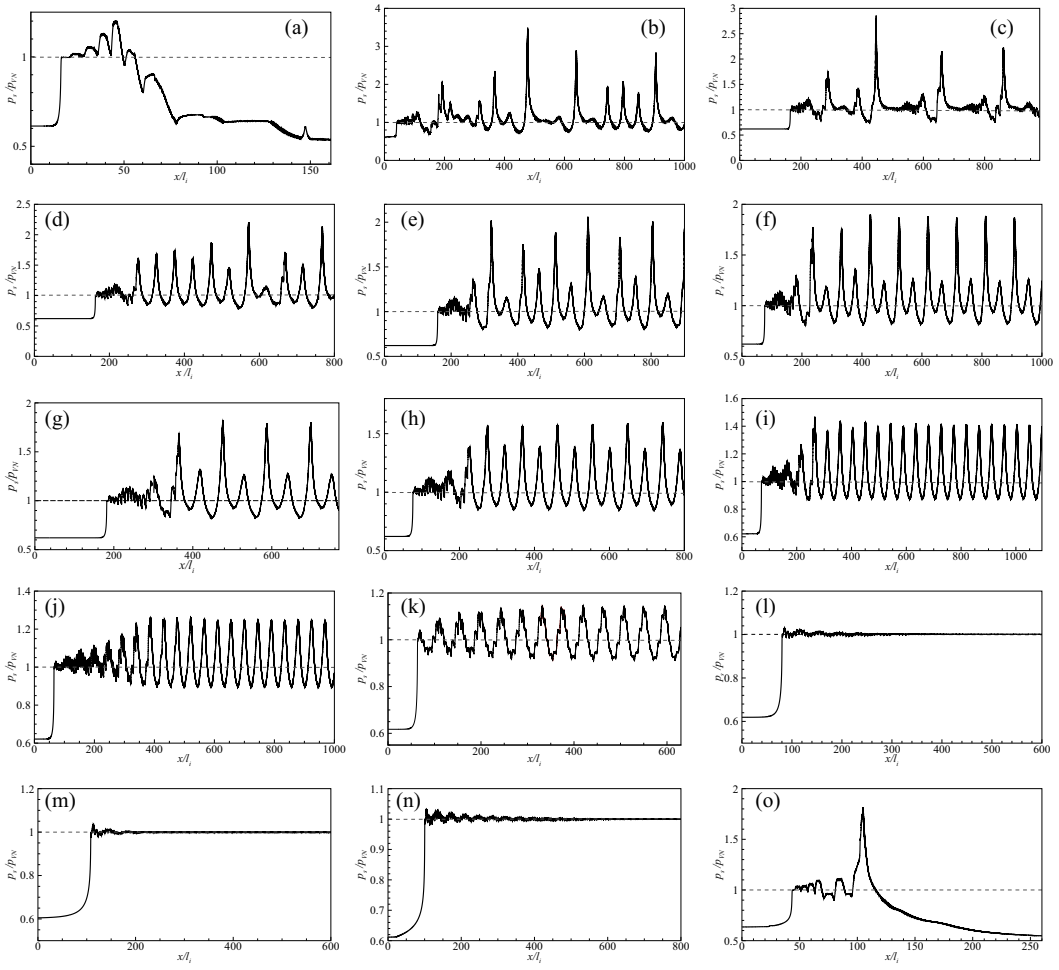

FIG. 4. Maximum pressure histories for different Ar dilutions: The region with low pressure is the steady ZND structure as initial condition; the induction length l_i corresponds to each Ar dilution, and p_{VN} is the steady von-Neumann value corresponding to each case.

different propagation modes for the different cases. It is seen that the detonation fails to sustain after several high-frequency oscillations for 15% Ar dilution. As the dilution increases, pulsation shifts from the chaotic mode to the stable mode. From 35% to 40% Ar dilution, detonation pulsations are chaotic, as shown in Figs. 4(b)–4(d). From 44% to 48%Ar dilutions, multiperiod modes are eventually formed; as Ar dilution increases, the minimum peak increases while the maximum peak decreases, as shown in Figs. 4(e)–4(g), showing that the pulsation tends to be regular. Single-period modes appear in the cases with 50%–58% Ar dilutions, as shown in Figs. 4(h)–4(j). For 65%–85% Ar dilutions, detonations tend to be stable after several small pulsations, as shown in Figs. 4(k)–4(l). As 90% Ar, the initially established detonation decays and quenches after a strong pressure pulse, showing that the detonability limit is reached and a sustaining propagation is not formed due to the low heat release rate for the large dilution.

Figure 4 shows that for 15% Ar the detonation fails to sustaining after several high-frequency oscillations, which is substantiated by complete decoupling of the leading shock with the reaction front at $x/l_i \sim 150$ shown in Figs. 5(a) and 5(b). The reaction zone in the detonation structure is rather short and the detonation is highly unstable for 15% Ar dilution. During the phase of

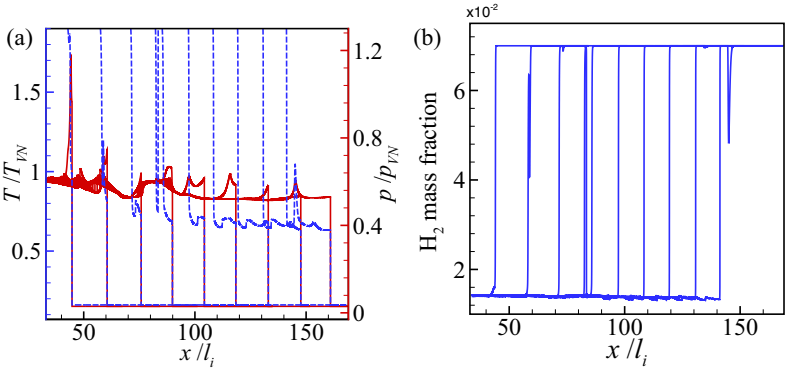

FIG. 5. Frontal structure in process of quenching detonation for 15% Ar dilution: $t = 0.396$, 0.54,0.63, 0.765, 0.899, 1.01, 1.15, 1.29, 1.41 μs. T_{VN} is the steady von-Neumann value.

decay, bulk unreacted gas escapes from the leading shock and is left behind the front, leading to failure of the propagation. Investigation of the reaction zone structure during the decay revealed that failure occurs due to highly pulsating instability. When the post-shock temperature decays below $\sim 0.7T_{VN}$, the reaction rate is found to be too slow to maintain the coupling with the exothermic part of the reaction zone that is required to drive the wave. As a result, the reaction layer then completely decouples from the shock and the detonation quenches. This failure scenario was previously observed and studied by Short *et al.* [17] in their numerical simulations using a simplified three-step chain-branching reaction scheme. Consequently, for 1D detonation at a global CJ speed, there is also a limiting behavior at 15% Ar dilution because the instability can kill a formed detonation.

Figure 6 shows the evolution of front structure in decay of the detonation for 90%Ar dilution. It is seen that after several high-frequency oscillations a strong pulse appears and an overdriven detonation forms, with a peak pressure of $\sim 1.8\, p_{VN}$. After the strong pulse, the overdriven detonation decays significantly and the main reaction layer recedes from the leading shock, resulting in long induction zone with a temperature gradient. However, as it decays below the CJ state, a fast flame in the high-temperature region fails to accelerate and cannot catch up with the leading shock due to low heat release rate caused by the large dilution, although it propagates in the temperature gradient. The measured speed of the leading shock wave is ~ 1.2 (964.9 m/s), while the speed of the reaction front is ~ 0.8(660.4 m/s) at $x/l_i \sim 250-350$. The shock temperature and pressure are 939.8 K and 9.1 atm respectively, and the corresponding autoignition time of the shocked gas is so

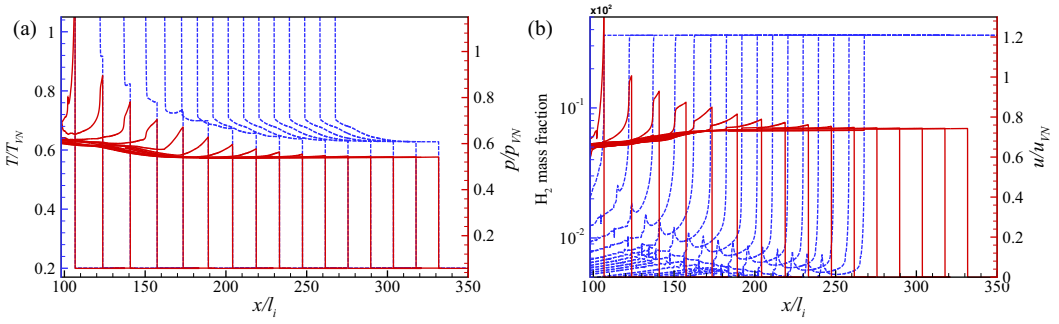

FIG. 6. Frontal structure in process of quenching detonation for 90% Ar dilution: $t = 67.75$, 84.6, 104.11, 124.51, 144.9, 165.3, 185.7, 207.0, 224.7, 245.1, 266.4, 285.9, 305.4, 324.9, 346.2, and 368.4 μs.

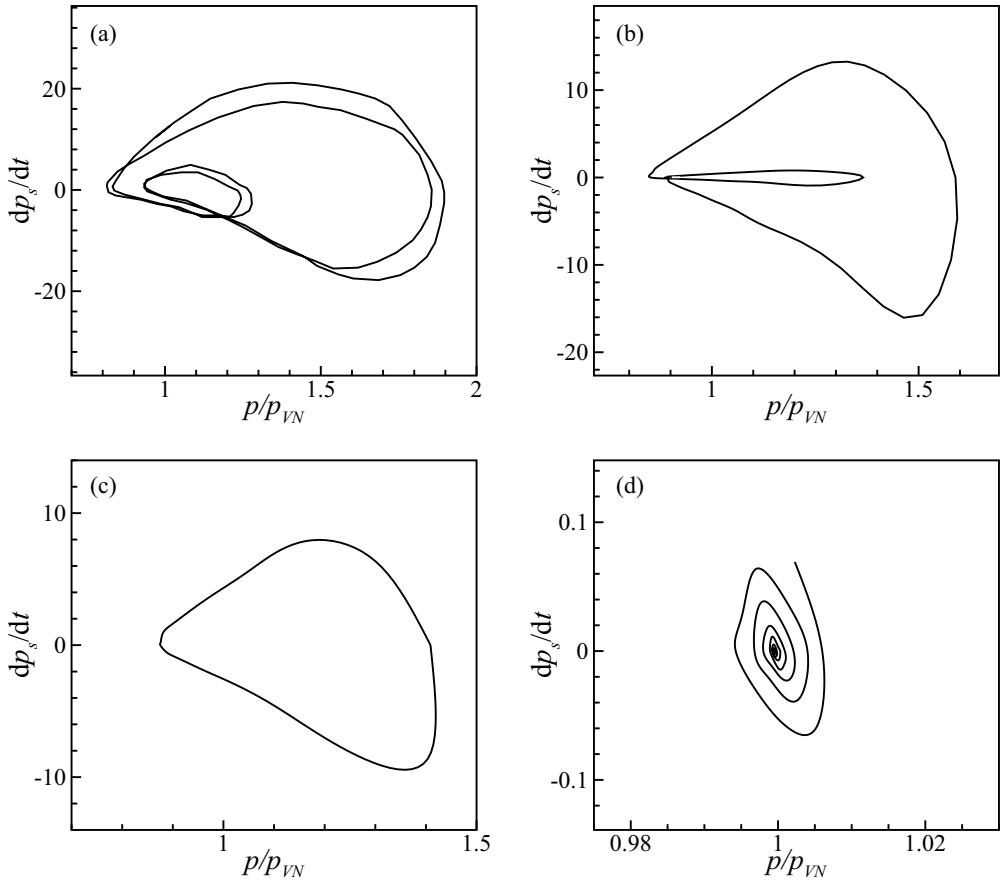

FIG. 7. Phase space plot for different Ar dilutions: (a) 45% Ar, (b) 48% Ar, (c) 50% Ar, and (d) 75% Ar.

long that reinitiation does not happen. Furthermore, unreacted H_2 fuel shown by H_2 mass fraction in Fig. 6(b) is observed in decay of the overdriven detonation. For 90% Ar, the autoignition time is long and the heat release rate is low due to low shock temperature and pressure. In this manner, the coupling between the dynamical limit and the autoignition limit will produce the detonability limits.

In summary, three detonation modes, exhibiting stable, periodic, and chaotic behavior, have been identified with detailed reactions and by varying the mixture composition, similar to those reported by Sharpe and Falle [14] and Ng *et al.* [16]. The instability increases with the thermal sensitivity of the distribution of heat release, as is the case when decreasing the dilution. Modification of the ZND structure produced by Ar dilution is the cause of the 1D pulsating instability because the ignition delay time in shocked gas is changed. For 15% Ar dilution, strong instability leads to the failure of a sustaining detonation in the 1D problem, indicating that the detonation is near the limit of propagation. Furthermore, for the mixture with large dilution of 90% Ar, once the detonation decays to the minimum level where the chemical reaction rate is slow and the induction time is long, a very small quantity of heat release rate may make the reestablishment of detonation impossible. For the 1D limit Ar dilution, the corresponding 2D simulation will be presented latter.

Figure 7 shows phase space plots for periodical pulsation with 45% Ar, 48% Ar, 50% Ar, and 75% Ar, respectively. It is seen clearly that the four-lobe phase space is exhibited for 45% Ar, while the two-lobe phase space is observed for 48% Ar; the one-lobe phase space presents in the

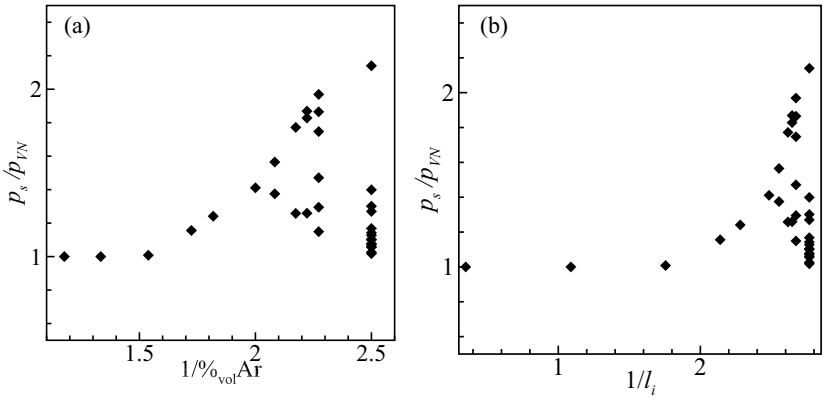

FIG. 8. Bifurcation diagram: peak shock pressure vs Ar dilution (a) and induction length (b).

single-period detonation with 50% Ar, while for 75% Ar there is no bounding of shock pressure and the curve gradually rotates to a point (steady shock pressure). It is seen that there are the maximum and minimum dp_s/dt during the compression and expansion phases of one pulsation respectively. During the compression phase, dp_s/dt rises and reaches the maximum, while, as the pressure is close to the peak, dp_s/dt is equal to zero. During the expansion phase, dp_s/dt is negative and the shocked pressure decreases to the minimum during one pulsation. It is observed that the phase space plots differ from that with the one-step reaction model [1]. This may be because the heat release rate for the one-step reaction model is not controlled as in real chemistry, in which the induction zone is not distinguished clearly from detonation structure. Consequently, the rate of change in shock pressure differs from that with the one-step reaction model, leading to the difference in phase space plots.

C. Bifurcation of pulsation for different Ar dilutions

Ng and Lee *et al.* [30] demonstrated that, for other parameters being fixed, there are two critical reduced activation energies with which to classify planar detonation into stable, unstable, and infinitely large-period modes, and pointed out that numerical simulations with detailed chemistry should be carried out for the study of phenomena observed with a one-step reaction model. The present results with detailed reactions for the H_2-O_2-Ar system show bifurcation diagrams, as shown in Figs. 8 and 9. The 1D detonations with real chemistry are classified into three classes. We observe that there exists a critical value between 65% and 50% Ar to transition from stable to single-period pulsation. The bifurcation point from single-period to period-doubling mode appears between 50% and 48% Ar; see Fig. 8(a). The bifurcation diagram related to the induction length is shown in Fig. 8(b).

For the detailed reaction mechanism, the bifurcation diagram with an effective activation energy is shown in Fig. 9. Conventionally, a reduced activation energy, E_a/R_uT_{VN}, can be obtained from an Arrhenius plot of $\ln(\tau)$ vs $1/T$, characterizing the temperature sensitivity of the induction time. For a one-step reaction model or an elementary reaction with a single activation energy, the result is

$$\ln(\tau) = \frac{E_a}{R_uT} + \text{constant}.$$

For multistep kinetics, the reduced activation energy E_a/R_uT_{VN} can be determined by

$$\frac{E_a}{R_uT_{VN}} = \frac{1}{T_{VN}}[\ln(\tau^+) - \ln(\tau^-)] \Big/ \left(\frac{1}{T^+} - \frac{1}{T^-}\right).$$

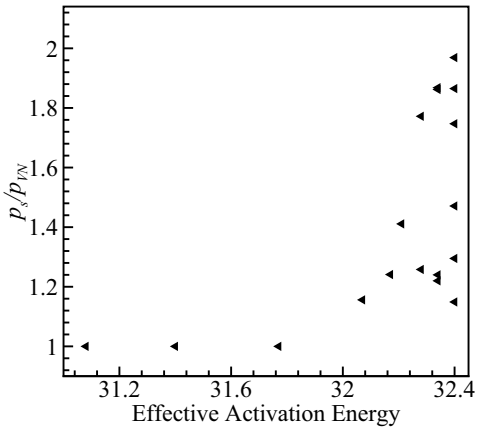

FIG. 9. Bifurcation diagram indicated by shock pressure as a function of effective activation energy.

Here T^+ and T^- bracket T_{VN}, i.e., $T^{\pm} = T_{VN} \times (1 \pm 0.01)$, and τ^+ and $\tau^-$are the corresponding induction times [31–33]. It is calculated that the stability boundary is between 31.76 and 32.08, and the bifurcation of period doubling is approximately 32.2 in the present diagram.

The curves of the stability parameter, $\chi = E_a/RT_{VN} \times l_i/l_R$, are shown in Fig. 10. Generally, it is demonstrated that Ng's criterion [16] works for prediction of the 1D detonation instability for the H_2-O_2 system with different Ar dilutions.

D. Detonation limits

From above discussion, it is found that the detonability limit is at 90% Ar dilution for propagation starting from a steady 1D detonation at the global CJ state. However, if it can be initiated directly by the source energy, a blasting cap is required for a highly Ar diluted mixture. Therefore, we carry out the simulation of a direct initiation to identify the detonation limit of 90% Ar through an evolution from a strong source energy ($p = 10$ atm, $T = 2100$ K in the initiation region). Figure 11 shows that a strongly overdriven detonation can be produced by a high source energy, and then it decays to a CJ state and triggers a strong pulse, demonstrating that a successful initiation can be formed. After undergoing the strong pulse, a formed detonation fails to sustain. In the corresponding 2D

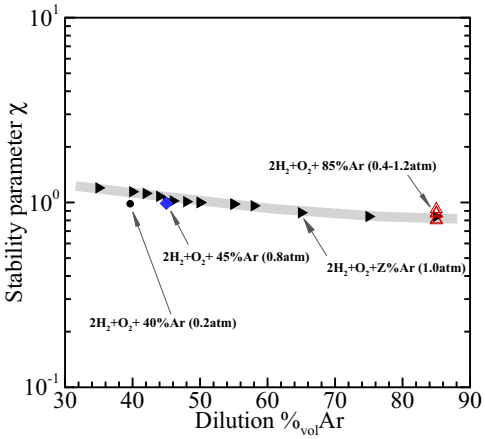

FIG. 10. Stability factor χ as a function of dilution.

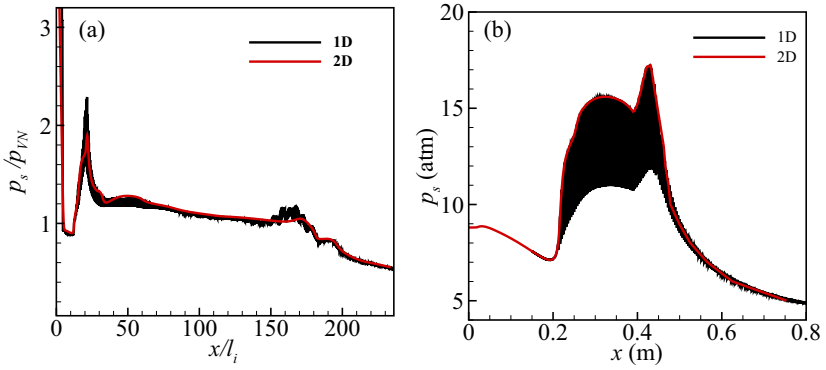

FIG. 11. Initiation led by high energy source (a) and induced temperature gradient (b) for 90% Ar. The black shaded region in (b) is caused by longitudinal and high-frequency oscillation of shock pressure for the 1D case.

case, eventually the detonation still does not sustain, as substantiated by the maximum pressure in Fig. 11. Consequently, for 90% Ar, failure happens again for a direct initiation from a strong source energy. Furthermore, we study the detonation initiation by setting a temperature gradient to identify whether a detonation eventually quenches. Due to the gradient mechanism, a detonation can be triggered. A strongly overdriven detonation is formed in the region with the temperature gradient. When the detonation goes out of the region with the gradient, it undergoes a strong pulse and then decays and eventually quenches in the uniform region. This also substantiates that the detonation limit is at 90% Ar dilution.

Radulescu *et al.* [18] demonstrated that a highly unstable detonation in 1D simulation was prone to failure to survive for a highly active mixture. The present simulations show that, as Ar dilution decreases to 15% Ar, the detonation becomes more unstable and cannot sustain. It is interest to identify whether there is a limiting behavior at 15% Ar dilution. Hence, we select 15% Ar dilution to carry out 1D and 2D simulations with a grid resolution of 1×10^{-6} mm (60 pts/$l_{1/2}$), identifying the propagation of 1D and 2D detonations produced by a subcritical direct initiation with $T = 2100$ K and $p = 4$ atm. For the 1D case, the detonation wave decays from the initial overdriven to the CJ state and undergoes a low-velocity phase. During the low-velocity phase, the leading shock decays. Although the leading shock decays below approximately $0.8p_{VN}$, it can reinitiate unreacted gas to form a detonation, with a pressure pulse at $x/l_i \sim 70$; subsequently it decays again below $\sim 0.6\, p_{VN}$ at $x/l_i \sim 140$ and quenches eventually. This demonstrates that the 1D initiation fails via subcritical initiation; see the black line in Fig. 12(a). However, for 2D instability, a cellular detonation appears at $x/l_i \sim 50$ and sustains, with irregular cells shown in Fig. 12(b). Consequently, the initiation fails in the 1D simulation, while it succeeds in the 2D case, demonstrating that cellular instability is beneficial for sustaining a detonation in the confinement domain.

In summary, using the realistic chemical kinetic model for H_2-O_2 mixtures, the present numerical results indicate that for 15% Ar dilution the 1D pulsating detonation cannot sustain due to high instability, while the 2D cellular detonation can sustain. In the 1D detonation, ignition can only be achieved via adiabatic shock induction. Therefore, there are no other mechanisms to effect ignition. However, in multidimensional detonations, ignition behind the strong transverse shocks, by transverse wave interactions and turbulent mixing, can provide alternate means to effect autoignition and thus maintain the detonation propagation. The role of transverse waves thus becomes essential to sustain the detonation propagation for highly unstable detonations [34,35]. For 15% Ar dilution, transverse waves play an important role in self-sustaining propagation in the confined domain; the detonation always fails when transverse waves are eliminated [35]. In unconfined space, as the role of transverse waves weakens and the reamplification of transverse waves disappears, it is more difficult to sustain a cellular detonation [36].

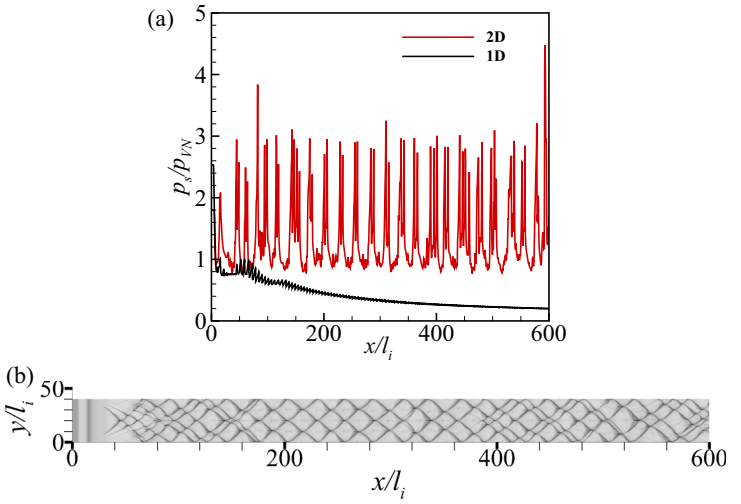

FIG. 12. 1D and 2D initiation by a subcritical way for 15% Ar dilution: (a) red line is maximum pressure history along the center of the 2D domain; (b) cellular feature.

V. CONCLUSIONS

The structure and propagation of one-dimensional (1D) detonations are investigated by high-resolution simulation for the H_2-O_2 system with different Ar dilutions. Three detonation modes are observed, namely the highly unstable, chaotic detonation, the mildly unstable detonation with either multi- or single-period pulsations, and the stable detonation. As Ar dilution increases, the detonability limit is found, which is caused by low heat release rate due to the dilution effect. The bifurcation diagram of 1D detonation instability is established, and the global bifurcation diagram is similar to that by the one-step model. Eventually, the numerical results demonstrate that for real chemistry the criterion of Ng *et al.* [16] still works well for prediction of 1D detonation instability. Ng *et al.* [16] studied the pulsating instability of 1D detonation for different reaction parameters in a two-step simplified model, and established a bifurcation diagram as a parameter controlling a reaction time in the model. It is of interest to compare the present results with the two-step and three-step models in future work.

ACKNOWLEDGMENTS

This research is supported by the National Natural Science Foundation of China under Grants No. 11972090 and No. 11732003, and by the Science and Technology on Transient Impact Laboratory Foundation (Grant No. 6142606182104). The research is also supported by the European Commission for the Marie Curie International Fellowships Grant TurbDDT (Grant No. 793072).

[1] J. H. S. Lee, *The Detonation Phenomena* (Cambridge University Press, Cambridge, 2008).

[2] P. Clavin and L. T. He, Stability and nonlinear dynamics of one dimensional overdriven detonations in gases, J. Fluid Mech. **306**, 353 (1996).

[3] P. Clavin and B. Denet, Diamond Patterns in Cellular Fronts of Overdriven Detonation, Phys. Rev. Lett. **88**, 044502 (2002).

[4] P. Clavin, L. He, and F. A. Williams, Multidimensional stability analysis of overdriven gaseous detonations, Phys. Fluids **9**, 3764 (1997).

[5] G. Lodato, L. Vervisch, and P. Clavin, Direct numerical simulation of shock wavy-wall interaction: Analysis of cellular shock structure and flow patterns, J. Fluid Mech. **789**, 221 (2016).
[6] J. B. McVey and T. Y. Toong, Mechanism of instabilities of exothermic hypersonic blunt body flows, Combust. Sci. Technol. **3**, 63 (1971).
[7] A. Matsuo, K. Fujii, and T. Fujiwara, Flow features of shock-induced combustion around projectile traveling at hypervelocities, AIAA J. **33**, 1056 (1995).
[8] H. I. Lee and D. S. Stewart, Calculation of linear detonation instability-one-dimensional instability of plane detonation, J. Fluid Mech. **216**, 103 (1990).
[9] M. Short, A. K. Kapila, and J. J. Quirk, The chemical-gas dynamic mechanisms of pulsating detonation wave instability, Philos. Trans. R. Soc. London A **357**, 3621 (1999).
[10] M. Short and G. J. Sharpe, Pulsating instability of detonations with a two-step chain-branching reaction model: Theory and numerics, Combust. Theor. Model. **7**, 401 (2003).
[11] C. Leung, M. I. Radulescu, and G. J. Sharpe, Characteristics analysis of the one-dimensional pulsating dynamics of chain-branching detonations, Phys. Fluids **22**, 126101 (2010).
[12] P. Clavin and F. A. Williams, Dynamics of planar gaseous detonations near Chapman-Jouguet conditions for small heat release, Combust. Theor. Model. **6**, 127 (2002).
[13] L. He and J. H. S. Lee, The dynamical limit of one-dimensional detonations, Phys. Fluids **7**, 1151 (1995).
[14] G. J. Sharpe and S. A. E. G. Falle, One-dimensional numerical simulations of idealized detonations, Proc. R. Soc. London **455**, 1203 (1999).
[15] C. M. Romick, T. D. Aslam, and J. M. Powers, The effect of diffusion on the dynamics of unsteady detonations, J. Fluid Mech. **699**, 453 (2012).
[16] H. D. Ng, M. I. Radulescu, A. J. Higgins, N. Nikiforakis, and J. H. S. Lee, Numerical investigation of the instability for one-dimensional Chapman-Jouguet detonations with chain-branching kinetics, Combust. Theor. Model. **9**, 385 (2005).
[17] M. Short and J. J. Quirk, On the nonlinear stability and detonability limit of a detonation wave for a model three-step chain-branching reaction, J. Fluid Mech. **339**, 89 (1997).
[18] M. I. Radulescu, H. D. Ng, J. H. S. Lee, and B. Varatharajan, The effect of argon dilution on the stability of acetylene-oxygen detonations, Proc. Combust. Inst. **29**, 2825 (2002).
[19] S. Yungster and K. Radhakrishan, Pulsating one-dimensional detonations in hydrogen-air mixtures, Combust. Theor. Model. **8**, 745 (2004).
[20] C. M. Romick, T. D. Aslam, and J. M. Powers, Verified and validated calculation of unsteady dynamics of viscous hydrogen-air detonations, J. Fluid Mech. **769**, 154 (2015).
[21] J. M. Powers and S. Paolucci, Accurate spatial resolution estimates for reactive supersonic flow with detailed chemistry, AIAA J. **43**, 1088 (2005).
[22] J. L. Ziegler, R. Deiterding, J. E. Shepherd, and D. I. Pullin, An adaptive high-order hybrid scheme for compressive, viscous flows with detailed chemistry, J. Comput. Phys. **230**, 7598 (2011).
[23] M. A. Sussman, Numerical simulation of shock-induced combustion, Ph.D. thesis, Stanford University (1995).
[24] R. J. Kee, F. M. Rupley, and J. A. Miller, Chemkin II: A Fortran chemical kinetics package for the analysis of gas phase chemical kinetics, Sandia National Laboratories Technical Report No. SAND89-8009B (1992).
[25] R. J. Kee, G. Dixon-Lewis, J. Warnatz, M. E. Coltrin, and J. A. Miller, A Fortran computer code package for the evaluation of gas-phase multi-component transport properties, Sandia National Laboratories Technical Report No. SAND86-8246 (1991).
[26] A. L. Sánchez and F. A. Williams, Recent advances in understanding of flammability characteristics of hydrogen, Prog. Energ. Combust. **41**, 1 (2014).
[27] G. S. Jiang and C. W. Shu, Efficient implementation of weighted ENO schemes, J. Comput. Phys. **126**, 202 (1996).
[28] C. A. Kennedy and M. H. Carpenter, Additive Runge-Kutta schemes for convection diffusion reaction equations, Appl. Numer. Math. **44**, 139 (2003).
[29] C. Wang, C. W. Shu, W. H. Han, and J. G. Ning, High resolution WENO simulation of 3D detonation waves, Combust. Flame **160**, 447 (2013).

[30] H. D. Ng, A. J. Higgins, C. B. Kiyanda, M. I. Radulescu, J. H. S. Lee, K. R. Bates, and N. Nikiforakis, Nonlinear dynamics and chaos analysis of one-dimensional pulsating detonations, Combust. Theor. Model. **9**, 159 (2005).

[31] J. M. Austin, F. Pintgen, and J. E. Shepherd, Reaction zones in highly unstable detonations, Proc. Combust. Inst. **30**, 1849 (2005).

[32] F. Pintgen and J. E. Shepherd, Pulse detonation engine impulse analysis for partially-oxidized jet fuel, GALCIT Technical Report No. FM2003.001 (2003).

[33] E. Schultz and J. E. Shepherd, Validation of detailed reaction mechanisms for detonation simulation, GALCIT Technical Report No. FM99-5 (2000).

[34] A. Teodorczyk and J. H. S. Lee, Detonation attenuation by foams and wire meshes lining the walls, Shock Waves **4**, 225 (1995).

[35] M. I. Radulescu, The failure and initiation mechanism of detonations propagating in porous wall tubes, Ph.D. dissertation, McGill University, Montreal, Quebec (2002).

[36] W. H. Han, C. Wang, and C. K. Law, Pulsation in one-dimensional H_2-O_2 detonation with detailed reaction mechanism, Combust. Flame **200**, 242 (2019).